Stripe Noise Separation and Removal in Remote Sensing Images by Consideration of the Global Sparsity and Local Variational Properties

Xinxin Liu, Xiliang Lu, Huanfeng Shen, *Senior Member, IEEE*, Qiangqiang Yuan, *Member, IEEE*, Yuling Jiao, and Liangpei Zhang, *Senior Member, IEEE*

Abstract—Remote sensing images are often contaminated by varying degrees of stripes, which severely affects the visual quality and subsequent application of the data. Unlike with conventional methods, we achieve the destriping by separating the stripe component based on a full analysis of the various stripe properties. Under an optimization framework, an ℓ^0-norm-based regularization is used to characterize the global sparse distribution of the stripes. In addition, difference-based constraints are adopted to describe the local smoothness and discontinuity in the along-stripe and across-stripe directions, respectively. The alternating direction method of multipliers is applied to solve and accelerate the model optimization. Experiments with both simulated and real data demonstrate the effectiveness of the proposed model, in terms of both qualitative and quantitative perspectives.

Index Terms—Alternating direction method of multipliers (ADMM), destriping, optimization-based model, remote sensing image, sparsity.

I. INTRODUCTION

STRIPING effects are a common degrading phenomenon in spaceborne and airborne remote sensing imaging systems, from whiskbroom sensors [1], [2] to pushbroom scanners [3],

X. Liu is with the School of Resource and Environmental Sciences, Wuhan University, Wuhan 430079, China (e-mail: yuki_lxx@126.com).

X. Lu is with the School of Mathematics and Statistics and with the Computational Science Hubei Key Laboratory, Wuhan University, Wuhan 430072, China (e-mail: xllv.math@whu.edu.cn).

H. Shen is with the School of Resource and Environmental Sciences, with the Key Laboratory of Geographic Information System, Ministry of Education, and with the Collaborative Innovation Center of Geospatial Technology, Wuhan University, Wuhan 430079, China (e-mail: shenhf@whu.edu.cn).

Q. Yuan is with the School of Geodesy and Geomatics and with the Collaborative Innovation Center of Geospatial Technology, Wuhan University, Wuhan 430079, China (e-mail: yqiang86@gmail.com).

Y. Jiao is with the School of Statistics and Mathematics, Zhongnan University of Economics and Law, Wuhan 430073, China (e-mail: yulingjiaomath@whu.edu.cn).

L. Zhang is with the State Key Laboratory of Information Engineering in Surveying, Mapping, and Remote Sensing and with the Collaborative Innovation Center of Geospatial Technology, Wuhan University, Wuhan 430079, China (e-mail: zlp62@whu.edu.cn).

Color versions of one or more of the figures in this paper are available online at http://ieeexplore.ieee.org.

Digital Object Identifier 10.1109/TGRS.2015.2510418

[4]. Mainly because of the inconsistent responses between different detectors [2], the stripe noise can badly influence not only the visual appearance of the data but also the potential subsequent applications, such as classification, target detection, quantitative applications, and so on. In order to further improve the quality of remote sensing images, it is crucial to remove the stripe noise, while maintaining the original information of the healthy pixels.

To date, a large number of destriping algorithms have been proposed. In general, these methods can be categorized into several main groups. The first family of destriping approaches relies on the statistical properties of the data [4]–[10]. These methods assume similarity within the signal and then examine the distribution differences between each sensor for the purpose of adjusting the target distribution to the reference one. As typical examples, histogram modification [5], [6] and moment matching [7] are relatively early methods in the destriping field. Although these methods work with high efficiency, their performance is always unstable when the stripes are nonlinear and/or irregular. To address this problem, Shen *et al.* [10] proposed a piecewise approach based on local statistics, and Sun *et al.* [4] proposed a spectral moment method for hyperspectral images.

Filtering-based techniques, such as the Fourier domain filter [1], [2], [11], wavelet analysis [12], [13], and the combined wavelet-Fourier filter [14], [15], constitute another type of destriping method. These methods work by analyzing and truncating the specific stripe component in a transformed domain and can effectively handle the oblique stripes in georectified images. Since the periodic property of stripes can be easily identified in a power spectrum analysis and extracted from signals in a transformed domain, these filtering-based methods generally output better results for periodic stripe noise. Limited by the truncating step, more information than stripe noise is often filtered by the conventional methods [1], [2], [12], which can result in excessive destriping results with significant blurring or ringing artifacts, particularly when some stripelike details also exist in the observed data. To conquer this drawback, research has been undertaken [14], [15] to truncate stripe information more accurately in a transformed domain.

Recently, optimization-based models have attracted the attention of scholars and have become a popular group of destriping methods. Regarding the destriping issue as an ill-posed problem [16]–[20], these approaches make use of prior information to estimate the true image by minimizing the energy

function under a constraint term. For instance, Shen and Zhang [16] utilized a maximum *a posteriori* framework to solve the destriping and inpainting problem, supposing that normal pixels conform to the law of a Huber–Markov distribution. In [17], a more sophisticated algorithm was designed by taking the directional structural information of the stripe noise into account. Aiming at the simultaneous removal of random and stripe noise, a joint model combining unidirectional total variation and sparse representation was proposed in [18]. More recently, low-rank matrix recovery has been used to remove stripes in hyperspectral images [20]. Due to the flexibility of the optimization framework, it is a very promising approach with plenty of modeling space for the destriping problem.

To sum up, most of the current methods implement the destriping by directly estimating the latent clean images. This paper presents a different processing angle by estimating and separating the stripe component from the original noisy data. By analyzing and fully considering the characteristics of the stripes, we propose a method for stripe separation and removal under an optimization-based framework. Without the need to obtain the specific locations of the stripes in advance, both the global and local distributional characteristics of the stripe noise are carefully considered and applied in the proposed model. From the global perspective, the sparse property is first observed and then described based on an ℓ^0-norm-based functional term. As to the local level, the smoothness along the stripes and the discontinuity across the stripes are both analyzed and modeled in variational forms. In order to efficiently optimize the proposed model, an alternating direction method of multipliers (ADMM) approach is applied by decomposing the complex problem into some simpler subproblems.

The remainder of this paper is organized as follows: In Section II, the proposed model and the properties of stripe noise are introduced. The ADMM algorithm is described in Section III. In Section IV, the experimental results and a comparison with other methods are provided. Finally, the conclusions are drawn in Section V.

II. STRIPE SEPARATION AND REMOVAL MODEL

A. Problem Formulation

Assuming that the striping effects in remote sensing images can be considered as additive noise [17], [18], the degradation process can be written as

$$f_{x,y} = u_{x,y} + s_{x,y} \tag{1}$$

where $f_{x,y}$, $u_{x,y}$, and $s_{x,y}$ separately denote the actual data output from the detectors, the desired destriped data, and the stripe component at the location of (x, y). For simplicity, a matrix-vector form can be used to rewrite (1) as follows:

$$\mathbf{f} = \mathbf{u} + \mathbf{s}. \tag{2}$$

Here, $\mathbf{f}$, $\mathbf{u}$, and $\mathbf{s}$ represent the lexicographically ordered vectors of $f_{x,y}$, $u_{x,y}$, and $s_{x,y}$, respectively.

Generally speaking, most destriping models aim to directly estimate $\mathbf{u}$ from the given image $\mathbf{f}$. However, to further explore
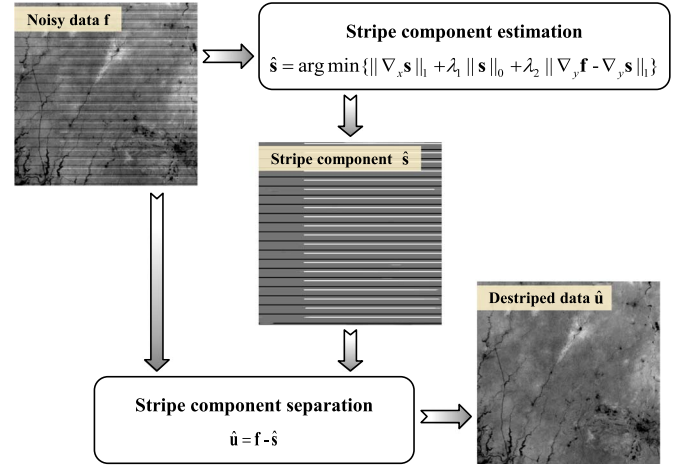

Fig. 1. Frame work of the proposed method.

the properties of stripe noise and design an effective destriping method with the ability to both remove noise and maintain healthy details, this paper first focuses on estimating an accurate stripe component.

Once $\hat{\mathbf{s}}$ is estimated, the desired image can be recovered by separating $\hat{\mathbf{s}}$ from the observed data $\mathbf{f}$, using the following expression:

$$\hat{\mathbf{u}} = \mathbf{f} - \hat{\mathbf{s}}. \tag{3}$$

The framework of the proposed method is illustrated in Fig. 1.

B. Proposed Model for Estimating the Stripe Component

Here, the key task is to explore the stripe properties, and to describe them in appropriate constraint terms to constitute an optimization model for the estimation of $\mathbf{s}$. More specifically, the global sparsity and the local variational properties in both the along-stripe and across-stripe directions are fully deliberated.

1) Global Sparsity: In recent years, sparse representation and sparsity promoting models have received a lot of attention and have been widely used in image restoration applications such as deblurring, denoising, and superresolution [21]–[23]. Other than utilizing special techniques to obtain the inner sparse property of images, the stripe component can be viewed as a kind of sparse matrix with a large number of zero elements in the stripe-free locations. This is due to the fact that the proportions of stripe noise in many remote sensing images are relatively low.

Considering the global sparse distributional property, it is natural for us to take advantage of this as a prior condition. As the ℓ^0-norm indicates the number of nonzero elements and encourages the sparsity, it fits well for the stripe property of sparse distribution. Therefore, we directly apply the ℓ^0-norm regularizer to the stripe matrix $\mathbf{s}$ as follows:

$$R_1(\mathbf{s}) = \|\mathbf{s}\|_0. \tag{4}$$

Here, the ℓ^0-norm plays an important role in controlling the process of noise extraction. To be more specific, the stripe

component can be screened out avoiding extra background information loss under this kind of constraint, and thus, the pixels in the stripe-free areas remain relatively intact.

2) Local Smoothness in the Along-Stripe Direction: In general, from the local perspective, the inner pixels within a single stripe often have relatively small variations, which means that the stripe possesses good smoothness in the along-stripe direction. Since the difference reflects the variation between adjacent pixels, the smoothness can be effectively described by minimizing the partial difference along the stripe. Moreover, when taking the potential occurrence of nonlinear or irregular stripes [10] into account, the segmented stripe boundaries caused by varying degradation levels within a single stripe also need to be effectively preserved for an accurate estimation of the stripe component. To do this, we finally construct this term as

$$R_2(\mathbf{s}) = \|\nabla_x \mathbf{s}\|_1 \tag{5}$$

where ∇_x represents the partial differential operator in the along-stripe direction. Due to its ability to accept huge jumps [24] in $\|\nabla_x \mathbf{s}\|_1$, the ℓ^1-norm regularization fits better than the ℓ^2-norm regularization in describing the along-stripe smoothness, while simultaneously preserving the segmented stripe boundaries.

3) Local Discontinuity in the Across-Stripe Direction: In addition to the smoothness along the stripes, the discontinuity across the stripes is also a very important local property. For example, the difference in the across-stripe direction often has a large absolute value at the stripe locations and a small value at the nonstripe locations. Although the differential values vary a lot, it is still difficult to accurately extract stripe pixels from the whole image using a threshold. Considering the fact that the partial differential result of the original image can reflect the actual across-stripe difference of each pixel, it is natural to use this information as a reference to help determine the discontinuity of the stripes. Accordingly, we have designed the following expression:

$$R_3(\mathbf{s}) = \|\nabla_y \mathbf{f} - \nabla_y \mathbf{s}\|_1 \tag{6}$$

where ∇_y is the partial differential operator in the across-stripe direction. General speaking, the ℓ^2-norm is a common choice to ensure that $\nabla_y \mathbf{s}$ is similar to $\nabla_y \mathbf{f}$ by penalizing the variations between $\nabla_y \mathbf{f}$ and $\nabla_y \mathbf{s}$. However, to ensure that the differential information across the stripe from observed data $\mathbf{f}$ can be more accurately mapped to the stripe component $\mathbf{s}$, the ℓ^1-norm is finally chosen. Furthermore, from a different point of view, the function of $R_3(\mathbf{s})$ is also equal to minimizing the across-stripe difference of the latent image for $\nabla_y \mathbf{f} - \nabla_y \mathbf{s} = \nabla_y \mathbf{u}$.

After fully analyzing the stripe noise from both the global and local perspectives, we can summarize its three typical distributional properties of sparsity, smoothness (along the stripes), and discontinuity (across the stripes). By combining these properties, a unified framework to solve the stripe component can be constructed as follows:

$$\hat{\mathbf{s}} = \arg\min \left\{ \|\nabla_x \mathbf{s}\|_1 + \lambda_1 \|\mathbf{s}\|_0 + \lambda_2 \|\nabla_y \mathbf{f} - \nabla_y \mathbf{s}\|_1 \right\} \tag{7}$$

where λ_1 and λ_2 are two parameters to balance the constraining degree of the different terms.

III. ADMM OPTIMIZATION

Due to the nondifferentiability and inseparability of the proposed model (7), it is necessary to find an efficient solution to tackle this nonsmooth and nonconvex optimization problem. Recently, the ADMM algorithm, which is well suited to distributed convex optimization, has become a powerful approach for many problems, such as ℓ^1 minimization and total variation (TV) minimization in image processing [25]–[27]. Since the ADMM approach combines the benefits of the decomposability in dual ascent and the superior convergence properties of the method of multipliers [28]–[30], it is competitive when compared to many of the state-of-the-art methods for constrained optimization. Therefore, in this paper, we adopt the ADMM approach to minimize the proposed destriping model in (7).

By introducing three auxiliary variables $\mathbf{Y}$, $\mathbf{H}$, and $\mathbf{W}$, we first convert the unconstrained minimization problem (7) into a constrained one, as follows:

$$\min \left\{ \|\mathbf{Y}\|_1 + \lambda_1 \|\mathbf{H}\|_0 + \lambda_2 \|\mathbf{W}\|_1 \right\}$$
$$\text{s.t. } \mathbf{Y} = \nabla_x \mathbf{s}, \ \mathbf{H} = \mathbf{s}, \ \mathbf{W} = \nabla_y \mathbf{f} - \nabla_y \mathbf{s}. \tag{8}$$

As in the method of multipliers, we then form the augmented Lagrangian as follows:

$$\mathcal{L}(\mathbf{Y}, \mathbf{H}, \mathbf{W}, \mathbf{s}, p_1, p_2, p_3)$$
$$= \|\mathbf{Y}\|_1 + \lambda_1 \|\mathbf{H}\|_0 + \lambda_2 \|\mathbf{W}\|_1 + p_1^T (\nabla_x \mathbf{s} - \mathbf{Y})$$
$$+ p_2^T (\mathbf{s} - \mathbf{H}) + p_3^T (\nabla_y \mathbf{f} - \nabla_y \mathbf{s} - \mathbf{W}) + \frac{\rho_1}{2} \|\nabla_x \mathbf{s} - \mathbf{Y}\|_2^2$$
$$+ \frac{\rho_2}{2} \|\mathbf{s} - \mathbf{H}\|_2^2 + \frac{\rho_3}{2} \|\nabla_y \mathbf{f} - \nabla_y \mathbf{s} - \mathbf{W}\|_2^2 \tag{9}$$

where p_1, p_2, and p_3 are Lagrange multipliers, and ρ_1, ρ_2, and ρ_3 represent the penalty parameters, which also determine the step sizes used to update the corresponding Lagrange multipliers. Each iteration of the ADMM can be decomposed into four simpler subproblems, and their variables are updated in an alternating and sequential way.

1) The $\mathbf{Y}$ subproblem is given by

$$\hat{\mathbf{Y}} = \arg\min \left\{ \|\mathbf{Y}\|_1 + p_1^T (\nabla_x \mathbf{s} - \mathbf{Y}) \right.$$
$$\left. + \frac{\rho_1}{2} \|\nabla_x \mathbf{s} - \mathbf{Y}\|_2^2 \right\} \tag{10}$$

which can be solved using a soft-threshold shrinkage operator [31] as follows:

$$\mathbf{Y}^{k+1} = S^{\ell^1} \left(\nabla_x \mathbf{s}^k + \frac{p_1^k}{\rho_1}, \frac{1}{\rho_1} \right) \tag{11}$$

where

$$S^{\ell^1}(x, T) = \begin{cases} x - T, & x > T \\ 0, & |x| \le T \\ x + T, & x < -T. \end{cases} \tag{12}$$

2) Similarly, the $\mathbf{W}$ subproblem reads

$$\hat{\mathbf{W}} = \arg\min \left\{ \lambda_2 \|\mathbf{W}\|_1 + p_3^T (\nabla_y \mathbf{f} - \nabla_y \mathbf{s} - \mathbf{W}) \right.$$
$$\left. + \frac{\rho_3}{2} \|\nabla_y \mathbf{f} - \nabla_y \mathbf{s} - \mathbf{W}\|_2^2 \right\} \quad (13)$$

and hence

$$\mathbf{W}^{k+1} = S^{\ell^1} \left(\nabla_y \mathbf{f} - \nabla_y \mathbf{s}^k + \frac{p_3^k}{\rho_3}, \frac{\lambda_2}{\rho_3} \right). \quad (14)$$

3) The $\mathbf{H}$ subproblem

$$\hat{\mathbf{H}} = \arg\min \left\{ \lambda_1 \|\mathbf{H}\|_0 + p_2^T (\mathbf{s} - \mathbf{H}) + \frac{\rho_2}{2} \|\mathbf{s} - \mathbf{H}\|_2^2 \right\} \quad (15)$$

has an explicit formula based on the hard-thresholding operator for the ℓ^0 penalty (see [32] and [33]). We can then update $\mathbf{H}^{k+1}$ as follows:

$$\mathbf{H}^{k+1} = S^{\ell^0} \left(\mathbf{s}^k + \frac{p_2^k}{\rho_2}, \sqrt{\frac{2\lambda_1}{\rho_2}} \right) \quad (16)$$

where

$$S^{\ell^0}(x, T) = \begin{cases} x, & |x| \geq T \\ 0, & |x| < T. \end{cases} \quad (17)$$

4) The $\mathbf{s}$ subproblem

$$\hat{\mathbf{s}} = \arg\min \left\{ p_1^T (\nabla_x \mathbf{s} - \mathbf{Y}) + p_2^T (\mathbf{s} - \mathbf{H}) \right.$$
$$+ p_3^T (\nabla_y \mathbf{f} - \nabla_y \mathbf{s} - \mathbf{W}) + \frac{\rho_1}{2} \|\nabla_x \mathbf{s} - \mathbf{Y}\|_2^2$$
$$\left. + \frac{\rho_2}{2} \|\mathbf{s} - \mathbf{H}\|_2^2 + \frac{\rho_3}{2} \|\nabla_y \mathbf{f} - \nabla_y \mathbf{s} - \mathbf{W}\|_2^2 \right\} \quad (18)$$

is a quadratic minimization problem. It has an explicit formula

$$\left(\rho_1 \nabla_x^T \nabla_x + \rho_2 + \rho_3 \nabla_y^T \nabla_y \right) \mathbf{s}^{k+1} = \rho_1 \nabla_x^T \left(\mathbf{Y}^{k+1} - \frac{p_1^k}{\rho_1} \right)$$
$$+ \rho_2 \left(\mathbf{H}^{k+1} - \frac{p_2^k}{\rho_2} \right) + \rho_3 \nabla_y^T \left(\nabla_y \mathbf{f} - \mathbf{W}^{k+1} + \frac{p_3^k}{\rho_3} \right) \quad (19)$$

which can be efficiently solved by fast Fourier transform (FFT).

Finally, in each iteration, the Lagrange multipliers p_1, p_2, and p_3 are updated as follows:

$$\begin{cases} p_1^{k+1} = p_1^k + \rho_1 (\nabla_x \mathbf{s}^{k+1} - \mathbf{Y}^{k+1}) \\ p_2^{k+1} = p_2^k + \rho_2 (\mathbf{s}^{k+1} - \mathbf{H}^{k+1}) \\ p_3^{k+1} = p_3^k + \rho_3 (\nabla_y \mathbf{f} - \nabla_y \mathbf{s}^{k+1} - \mathbf{W}^{k+1}). \end{cases} \quad (20)$$

Combining (11), (14), (16), (19), and (20), we have a one-step iteration for the ADMM. The ADMM decomposes the difficult minimization problem (7) into several easy subproblems. Specifically, the $\mathbf{Y}$ and $\mathbf{W}$ subproblems are solved by a soft-thresholding operator, whereas the $\mathbf{H}$ subproblem is solved by a hard-thresholding operator. For the $\mathbf{s}$ subproblem, FFT is utilized accordingly. In addition, the independent subproblems $\mathbf{Y}$, $\mathbf{H}$, and $\mathbf{W}$, along with their Lagrange multipliers p_1, p_2, and p_3, can be computed or updated in parallel. Finally, the proposed destriping model is summarized as Algorithm 1.

Algorithm 1: The proposed destriping algorithm

Input: data $\mathbf{f}$, parameters $\lambda_1, \lambda_2, \rho_1, \rho_2, \rho_3$.
Initialize: $\mathbf{s}_0 = \mathbf{0}$, $\mathbf{Y}_0 = \mathbf{0}$, $\mathbf{H}_0 = \mathbf{0}$, $\mathbf{W}_0 = \nabla_y \mathbf{f}$, $p_1 = \mathbf{0}$, $p_2 = \mathbf{0}$, $p_3 = \mathbf{0}$, and $\varepsilon = 10^{-4}$
  While ($\|(\mathbf{f} - \mathbf{s}^k) - (\mathbf{f} - \mathbf{s}^{k-1})\| / \|\mathbf{f} - \mathbf{s}^k\| > \varepsilon$ and $k < N_{\max}$) **do**
   Solve $\mathbf{Y}^{k+1}, \mathbf{W}^{k+1}, \mathbf{H}^{k+1}$ using a thresholding method by (11), (14), (16)
   Solve $\mathbf{s}^{k+1}$ using FFT by (19)
   Update the three Lagrange multipliers $p_1^{k+1}, p_2^{k+1}, p_3^{k+1}$ by (20)
  End While
Output: $\mathbf{u}^{k+1} = \mathbf{f} - \mathbf{s}^{k+1}$

IV. EXPERIMENTAL RESULTS AND DISCUSSION

To verify the effectiveness of the proposed destriping method, we undertook both simulated and real data experiments. Four state-of-the-art destriping methods that do not require the location information of the stripes were chosen for comparison: 1) combined wavelet-Fourier filtering (WAFT) [14]; 2) statistical linear destriping (SLD) [9]; 3) the unidirectional total variational model (UTV) [17]; and 4) the spatially adaptive unidirectional total variation model (SAUTV) [19]. For the quantitative evaluation of the different methods with different data, all the test images were normalized between [0, 1].

A. Simulated Data Experiments

In the simulated experiments, one 400×400 Terra MODIS subimage [see Fig. 2(a)] from a relatively homogeneous area and one 250×250 Hyperion subimage [see Fig. 3(a)] with complicated surface conditions were selected from their corresponding noise-free bands. In order to demonstrate the robustness of the proposed destriping method, we used linear degradation as the basic approach [7] and degraded the two test images in different ways.

For the Terra MODIS data, both whole stripes and part stripes were periodically added in the image. The width of the stripes was two lines, as shown in Fig. 2(b). Meanwhile, in the Hyperion data, we randomly chose 10% of the lines to add stripes. To make the situation more complicated, the degradation levels of the different stripes were also different [see Fig. 3(b)].
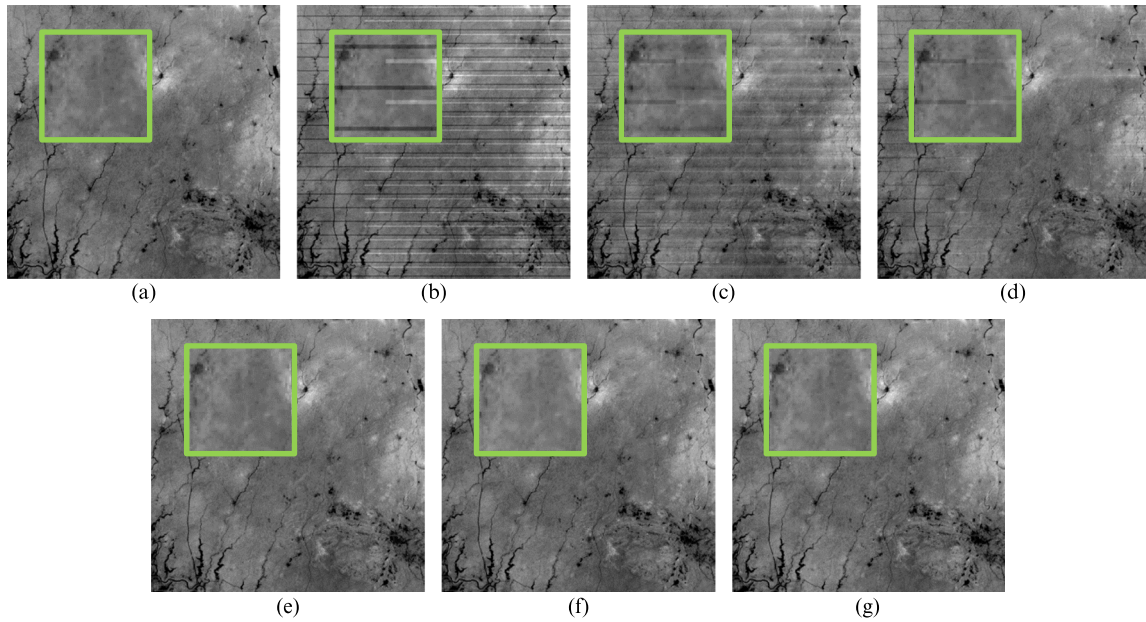
Fig. 2. Destriping results with the simulated Terra MODIS data: (a) original image; (b) degraded image with periodic stripes; (c) SLD; (d) WAFT; (e) UTV; (f) SAUTV; and (g) the proposed method.
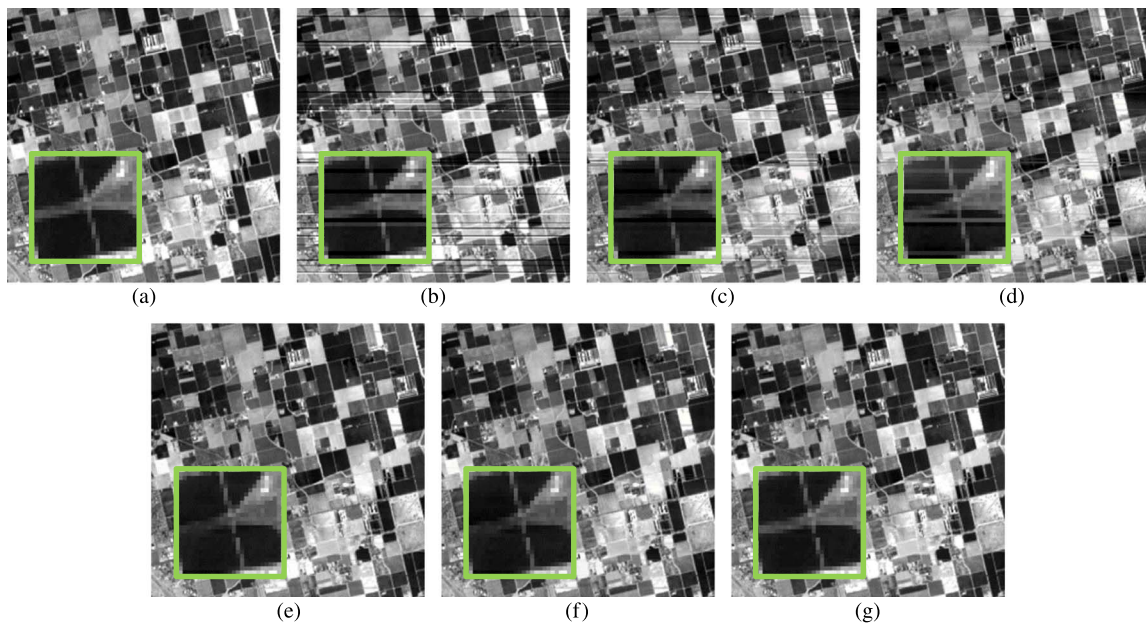

Fig. 3. Destriping results with the simulated Hyperion data: (a) original image; (b) degraded image with random stripes; (c) SLD; (d) WAFT; (e) UTV; (f) SAUTV; and (g) the proposed method.

Figs. 2 and 3 show the different destriping results for the simulated Terra MODIS and Hyperion data. As displayed in Figs. 2(c) and 3(c), the SLD method does a relatively poor job, with either obvious remaining stripes or some significant overcorrection. Although the results of the WAFT method in Figs. 2(d) and 3(d) contain fewer artifacts than SLD, its performance is still worse than UTV, SAUTV, and the proposed model. Although UTV, SAUTV, and the proposed method obtain comparative visual results for the periodic stripes in Fig. 2, the detail region in Fig. 3 reveals the difference. By fo-

cusing too much on smoothness, in the green mark of Fig. 3(e), some boundaries seem to be blurred after destriping by UTV. A similar visual result can be found in Fig. 3(f) for SAUTV. However, the proposed method, in contrast, shows a better visual performance in Fig. 3(g).

In order to test the abilities of the different methods to keep healthy pixels in the destriping process, the stripe components extracted from more complicated test data (Hyperion data) are given in Fig. 4. When compared to the actual added stripes in Fig. 4(a), it is clear that SLD, WAFT, and UTV all extract
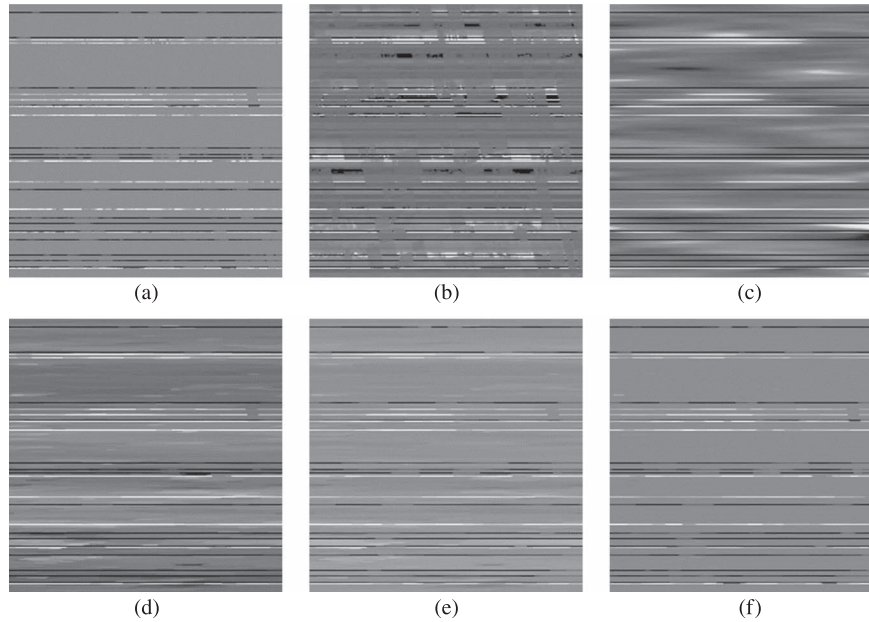
Fig. 4. Extracted stripe components for the Hyperion data: (a) the actual added stripes; (b) SLD; (c) WAFT; (d) UTV; (e) SAUTV; and (f) the proposed method.

additional background information in the stripe components, which results in significant data loss in the destriping results. Although the result of SAUTV in Fig. 4(e) is significantly improved, the extracted stripe component is still not as accurate as expected. In Fig. 4(f), it can be seen that the proposed method extracts not only the correct noise component but also the correct degradation level. Thus, in addition to suppressing the stripe noise successfully, the proposed method also has a much better ability to preserve healthy information.

Because of the availability of truth data in simulated experiments, both full-reference and nonreference indexes were used to give an overall quantitative assessment: the improvement factor (IF1) [34], the peak signal-to-noise ratio (PSNR), the structural similarity index (SSIM) [35], [36], the inverse coefficient of variation (ICV) [37], [38], and the mean relative deviation (MRD) [16]. Among them, ICV and MRD are nonreference indexes, and the others are full-reference indexes. IF1 was used to measure the image quality improvement after destriping, whereas PSNR and SSIM were utilized to assess the similarity between the reference and destriped images, which also reflects the models' ability to maintain useful information. For the nonreference indexes, ICV calculated in homogeneous regions was used to reflect the level of the remaining stripe noise, whereas MRD computed in noise-free sharp regions was used to evaluate the performance in retaining healthy details. In practice, the ICV and MRD indexes were separately calculated in homogeneous and heterogeneous regions within a 10×10 window. To decrease the influence of accidental factors, the mean ICV (MICV) of five homogeneous samples and the mean MRD (MMRD) of five heterogeneous samples were used to give the final evaluation. Generally speaking, better destriping results are reflected by higher IF1, PSNR, SSIM, and MICV values and lower MMRD values.

The quantitative assessment of the simulated experiments is shown in Table I. Here, it is clear that the proposed destriping

TABLE I
QUANTITATIVE ASSESSMENT OF THE SIMULATED DATA EXPERIMENTS

Images	Index	SLD	WAFT	UTV	SAUTV	Proposed
Terra MODIS	IF1	7.454	13.867	11.531	18.038	**28.876**
	PSNR	29.911	33.010	34.664	38.990	**42.403**
	SSIM	0.823	0.940	0.990	0.992	**0.998**
	MICV	13.653	17.065	18.916	18.107	**18.987**
	MMRD (%)	5.8	6.8	6.9	2.5	**0.0**
Hyperion	IF1	4.387	8.433	12.327	13.061	**26.618**
	PSNR	29.635	23.687	29.699	29.840	**33.595**
	SSIM	0.866	0.884	0.973	0.973	**0.986**
	MICV	6.030	12.900	25.187	24.311	**26.562**
	MMRD (%)	6.5	12.0	3.9	3.5	**0.2**

method outperforms the other four approaches, in terms of all these indexes, which is in accordance with the aforementioned visual evaluations.

B. Real Data Experiments

To further test the performance of the proposed method, four different kinds of real remote sensing images with different stripe noise distributions were used: 1) Aqua MODIS; 2) Terra MODIS; 3) Hyperspectral Digital Imagery Collection Experiment (HYDICE); and 4) Hyperion data. As typical examples of periodic stripes, band 30 of the Aqua MODIS data and band 28 of the Terra MODIS data (with the size of 400×400) extracted from their original versions were chosen as the experimental images. These data are available from http:// ladsweb.nascom.nasa.gov. For the random stripes, both band 87 of a 200×200 HYDICE urban subimage and band 56 of a 250×400 Hyperion subimage were selected to be tested. The original images can be downloaded online at http://www.tec. army.mil/hypercube and http://eo1.gsfc.nasa.gov, respectively.

It is shown that the MODIS data in Figs. 5(a) and 6(a) are highly contaminated by noisy periodic stripes [8]. In addition,
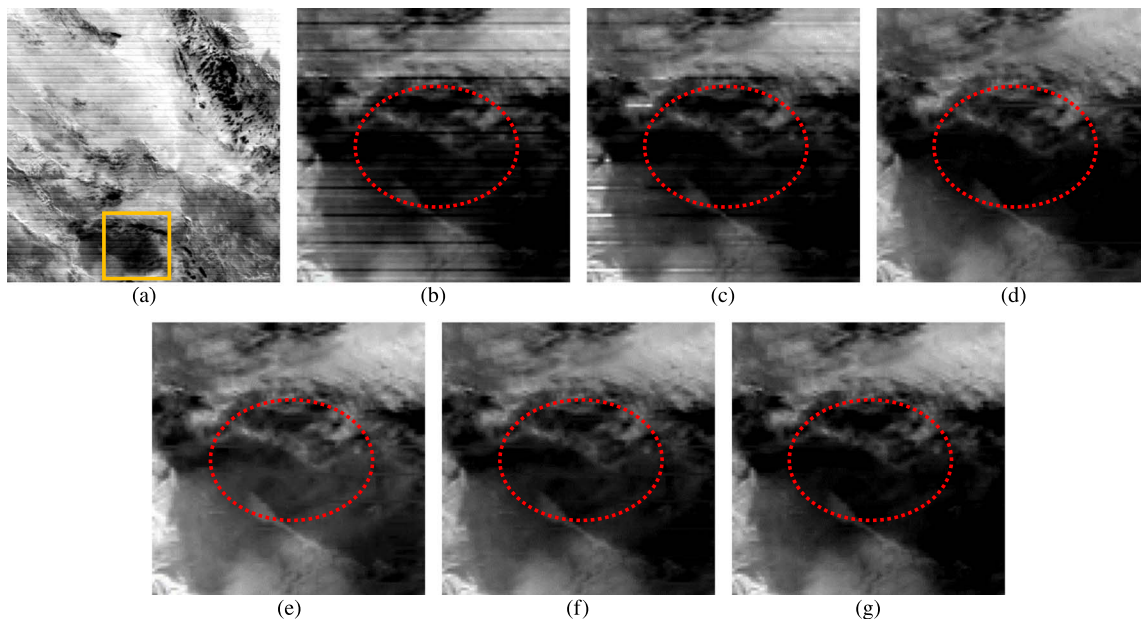
Fig. 5. Destriping results of Aqua MODIS band 30: (a) original image; (b) zoom of (a); (c) SLD; (d) WAFT; (e) UTV; (f) SAUTV; and (g) the proposed method.
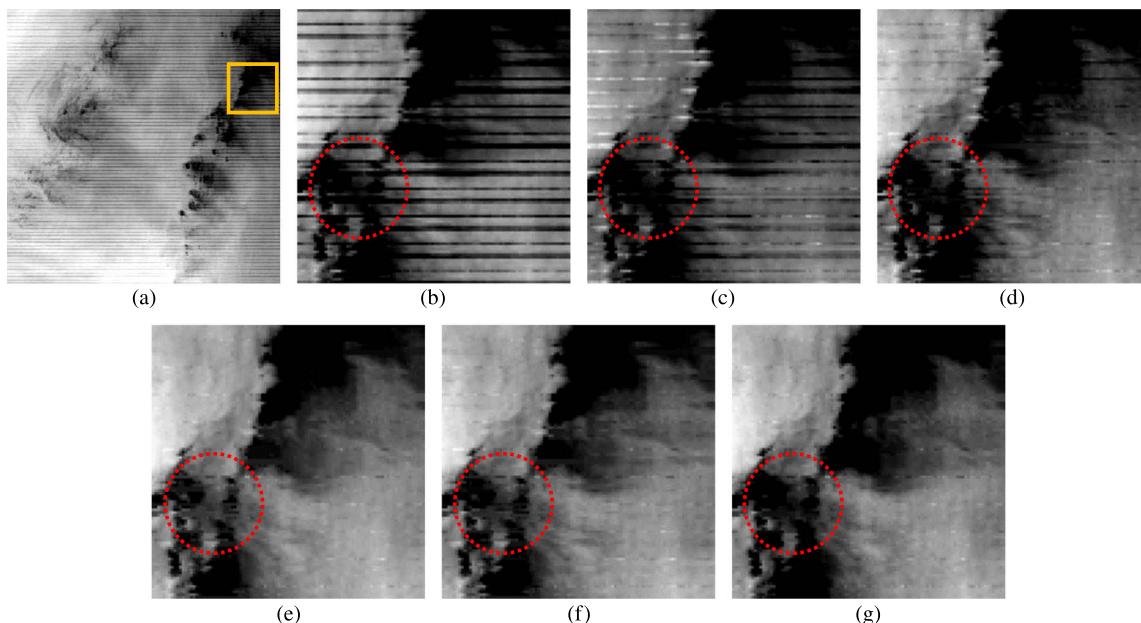

Fig. 6. Destriping results of Terra MODIS band 28: (a) original image; (b) zoom of (a); (c) SLD; (d) WAFT; (e) UTV; (f) SAUTV; and (g) the proposed method.

the ground-truth condition in the Aqua MODIS data is more complicated, whereas the noise level in the Terra MODIS data is much higher. In Figs. 7(a) and 8(a), the occurrences of stripe noise are much more irregular, with a random distribution over the whole or part of the image, respectively. Since the stripe noise is mainly concentrated in the left part of Fig. 8(a), this image is particularly suitable to test the ability of the different destriping methods to preserve healthy information.

Figs. 5–8 present the destriping results of SLD, WAFT, UTV, SAUTV, and the proposed method. A visual assessment of these results clearly shows that the proposed approach can effectively remove different types of stripe noise. According to

the destriping results of WAFT and SLD, these two methods are not as robust as the proposed method because satisfactory results are only obtained for certain images. Taking Fig. 6(d) as an example, the artifacts caused by WAFT are obvious on the homogeneous background. In addition, the residual stripes in the SLD-recovered results, such as Figs. 6(c) and 8(c), are also significant. Although the visual results of UTV seem plausible, we still have to consider its oversmoothing effect. For instance, in the MODIS data, UTV focuses too much on the smoothing and leads to local brightness distortion, as shown in Figs. 5(e) and 6(e). SAUTV attempts to deal with the oversmoothing effect of UTV; however, the actual results in Figs. 5(f) and 6(f)
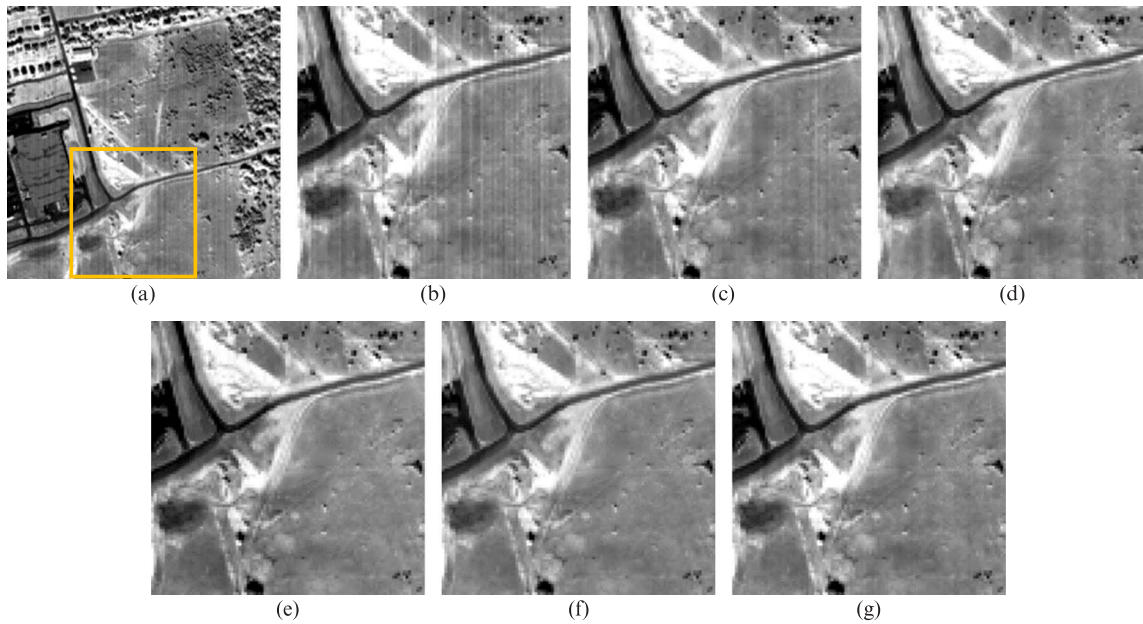
Fig. 7. Destriping results of HYDICE band 87: (a) original image; (b) zoom of (a); (c) SLD; (d) WAFT; (e) UTV; (f) SAUTV; and (g) the proposed method.
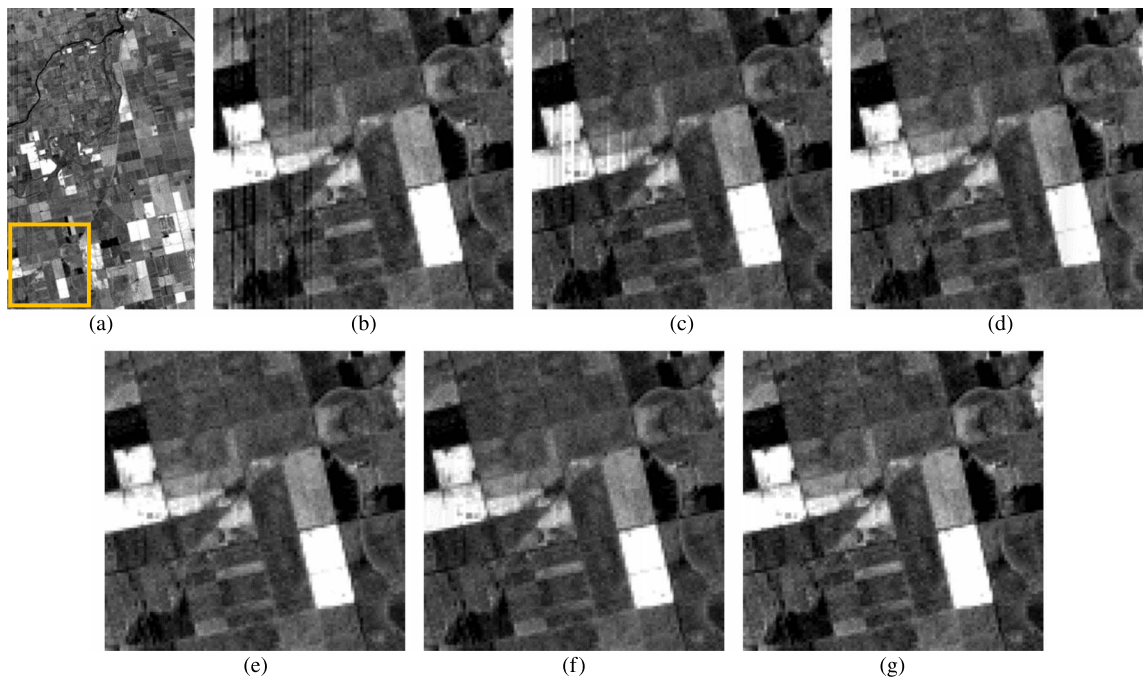

Fig. 8. Destriping results of Hyperion band 56: (a) original image; (b) zoom of (a); (c) SLD; (d) WAFT; (e) UTV; (f) SAUTV; and (g) the proposed method.

reveal its limitation, since SAUTV alleviates but does not eliminate the brightness distortion.

The stripe noise separation results of the different methods for the different real data experiments are given in Fig. 9. Clearly, SLD, WAFT, UTV, and SAUTV all lose different degrees of useful information in the destriping process, whereas the proposed method separates and removes the noise component much more accurately. Moreover, Fig. 10 displays the mean cross-track profiles of Hyperion band 56. As the stripe noise in this data mostly occurs in the left part, the best mean

cross-track profile of the destriped image should be the same as the noisy image in the other nonstripe part. However, the corresponding profiles of SLD and WAFT in Fig. 10(b) and (c) differ a lot from Fig. 10(a) in the nonstripe part. In addition, UTV alleviates the fluctuation too much, which means that some fine details are simultaneously smoothed during the destriping process. A similar profile is output by SAUTV, as shown in Fig. 10(e). Unlike the four existing methods, the proposed approach can process random stripes, with the least amount of distortion, and is better able to preserve detailed information.
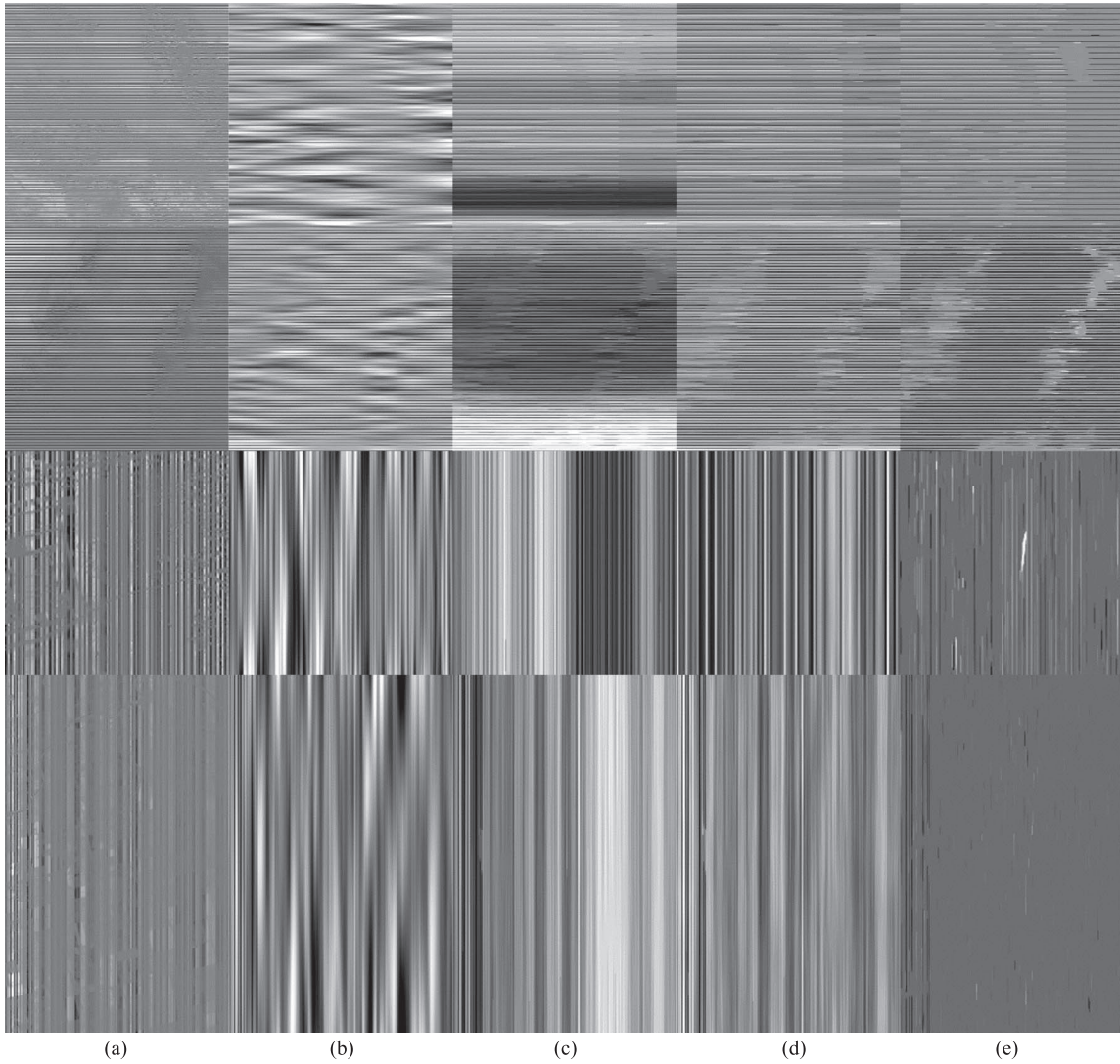
Fig. 9. Stripe components in Aqua MODIS band 30, Terra MODIS band 28, HYDICE band 87, and Hyperion band 56, extracted by: (a) SLD; (b) WAFT; (c) UTV; (d) SAUTV; and (e) the proposed method.
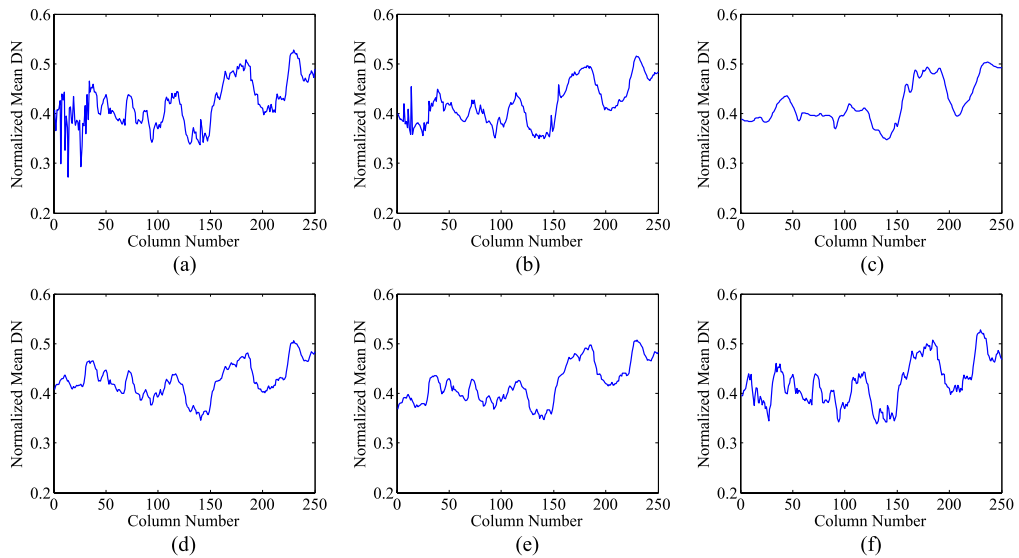

Fig. 10. Mean cross-track profiles of Hyperion band 56: (a) noisy image; (b) SLD; (c) WAFT; (d) UTV; (e) SAUTV; and (f) the proposed method.

TABLE II
QUANTITATIVE ASSESSMENT OF THE REAL DATA EXPERIMENTS

Images	Index	SLD	WAFT	UTV	SAUTV	Proposed
Aqua band	MICV	18.511	22.153	26.054	24.164	**26.417**
30	MMRD (%)	2.7	42.8	44.1	12.3	**0.8**
Terra band	MICV	16.805	47.615	47.628	43.931	**49.778**
28	MMRD (%)	19.6	11.0	33.20	12.7	**3.3**
HYDICE	MICV	13.594	14.345	15.803	16.149	**16.586**
band 87	MMRD (%)	4.6	6.8	13.7	7.1	**0.3**
Hyperion	MICV	6.891	8.286	9.265	8.517	**9.503**
band 56	MMRD (%)	3.6	7.6	5.0	4.0	**0.1**

For the quantitative evaluation, two nonreference indexes, i.e., MICV and MMRD, were used in the real data experiments. The specific calculation of MICV and MMRD was the same as in the simulated experiments, and the results are listed in Table II. Here, it can be seen that the proposed method simultaneously obtains the highest MICV values and the lowest MMRD values in all the real data experiments, which confirms the effectiveness of the proposed method. If we only used MICV to evaluate the performances of the different methods, it could be inferred that UTV, SAUTV, and the proposed approach usually obtain similar results that are better than SLD and WAFT, which would suggest that these three methods have comparative destriping abilities. However, when taking the MMRD index into account, the advantage of the proposed method stands out in effectively preserving the original noise-free information.

C. Discussion

1) Parameter Selection: In this paper, the stripe distributional properties of sparsity, smoothness, and discontinuity are constructed as constraint terms to estimate the stripe component. Since the specific noise levels and proportions of stripes vary a lot, for a more accurate estimation, the different significances of these three properties also need to be carefully considered, i.e., the functioning degree of the corresponding constraint terms in model (7) need to be adjusted accordingly through the regularization parameters λ_1 and λ_2. Taking severe stripe noise as an example, its discontinuity would clearly stand out when compared to the other two distributional properties; thus, a larger λ_2 would be more helpful in this case. In addition, the proportion of the stripes is in close accordance with the sparsity. Specifically, the lower the proportion, the sparser the stripe component. Therefore, a higher λ_1 would be more suitable for a sparser stripe situation. Due to the different degradation levels of the test images in our experiments, the regularization parameters were set empirically with the range $[0.001, 0.01]$ for λ_1 and $[0.1, 1]$ for λ_2. Fortunately, in practical use, the sensor is usually a specific type, and its degradation level is relatively stable; hence, we can determine the values of the regularization parameters. However, at present, the regularization parameters cannot be automatically or adaptively chosen for different sensors, which will be further researched in our future work. For the penalty parameters, it can be seen that the choice of penalty parameter does not greatly affect the convergence of the ADMM algorithm [30]. To simplify the steps of the parameter adjustment, we empirically set $\rho_1 =$

TABLE III
RUNNING TIME(S) OF THE DIFFERENT METHODS
WITH TWO IMAGE SIZES

Image Size	SLD	WAFT	UTV	SAUTV	Proposed
250×250	0.458	0.170	11.992	11.171	1.630
400×400	0.851	0.192	54.436	54.726	6.108

$\rho_2 = \rho_3 = 100\lambda_2$. As to the parameters in the four compared methods, they were initially selected according to the authors' advice in the related papers, and they were further adjusted until they attained the best PSNR value in the simulated experiments or the best visual output in the real data experiments.

2) Running Time: Owing to the use of the ADMM algorithm, the independent subproblems $\mathbf{Y}, \mathbf{H}, \mathbf{W}$ and the three Lagrange multipliers in (20) can be calculated or updated in parallel. Moreover, to estimate the stripe component, the efficient FFT is chosen to solve the corresponding quadratic minimization problem in (19). Consequently, our optimization-based approach is relatively fast. The comparison of the running times of the different methods is given in Table III. All the experiments were conducted in MATLAB on a desktop personal computer with a 3.4-GHz CPU and 8-GB RAM.

3) Sparsity Explanation: Generally speaking, in most cases, the proportion of stripe noise in remote sensing images is relatively low, and the sparsity is quite significant. Under this circumstance, since the healthy pixels can be easily discriminated, the use of sparsity to screen out the stripe component is effective and necessary. Naturally, there will still be a few cases where the stripes are too dense to be considered as sparse noise. Although the sparsity has disappeared, the along-stripe smoothness and the across-stripe discontinuity will always be significant, and can be utilized to extract the stripe component. Although the extraction may not be as accurate as when the stripe noise is sparse, the result will still be acceptable for the reason that both the stripe pixels and healthy pixels are difficult to define in such a case. In addition, the output of the proposed method in such a case would be very close to or even equivalent to UTV.

V. CONCLUSION

In this paper, we have proposed a new destriping method taking the stripe noise properties of sparsity, smoothness, and discontinuity into full consideration. With the constraint of these properties, the model can lock the destriping process on noisy pixels and maintain the fine details of the original data. For the optimization, the ADMM method is applied to solve the corresponding optimization problem. Several simulated and real data sets were tested in our experiments. Both the qualitative and quantitative assessments confirmed that the proposed model can output better destriping results than the other state-of-the-art techniques of SLD, WAFT, UTV, and SAUTV. In addition, the proposed method is quite robust to most types of stripes, and it does not require the stripe positions in advance. As a result, it has good universality.

Although the proposed model works well on horizontal or vertical stripes, there are still limitations for oblique stripes in

georeferenced images. Thus, in the future, we will focus on the challenging task of the identification and subsequent removal of oblique stripes.

ACKNOWLEDGMENT

The authors would like to thank the four anonymous reviewers for their valuable comments.

REFERENCES

[1] J. J. Simpson, J. I. Gobat, and R. Frouin, "Improved destriping of GOES images using finite impulse response filters," *Remote Sens. Environ.*, vol. 52, no. 1, pp. 15–35, Apr. 1995.

[2] J. Chen, Y. Shao, H. Guo, W. Wang, and B. Zhu, "Destriping CMODIS data by power filtering," *IEEE Trans. Geosci. Remote Sens.*, vol. 41, no. 9, pp. 2119–2124, Sep. 2003.

[3] H. Jung, J. Won, M. Kang, and Y. Lee, "Detection and restoration of defective lines in the SPOT 4 SWIR band," *IEEE Trans. Image Process.*, vol. 19, no. 8, pp. 2143–2156, Aug. 2010.

[4] L. Sun, R. Neville, K. Staenz, and P. White, "Automatic destriping of Hyperion imagery based on spectral moment matching," *Can. J. Remote Sens.*, vol. 34, no. S1, pp. S68–S81, Jan. 2008.

[5] B. K. P. Horn and R. J. Woodham, "Destriping LANDSAT MSS images by histogram modification," *Comput. Graph. Image Process.*, vol. 10, pp. 69–83, May 1979.

[6] M. Wegener, "Destriping multiple sensor imagery by improved histogram matching," *Int. J. Remote Sens.*, vol. 11, no. 5, pp. 859–875, May 1990.

[7] F. L. Gadallah, G. Csillag, and E. J. M. Smith, "Destriping multisensory imagery with moment matching," *Int. J. Remote Sens.*, vol. 21, no. 12, pp. 2505–2511, Aug. 2000.

[8] P. Rakwatin, W. Takeuchi, and Y. Yasuoka, "Stripe noise reduction in MODIS data by combining histogram matching with facet filter," *IEEE Trans. Geosci. Remote Sens.*, vol. 45, no. 6, pp. 1844–1856, Jun. 2007.

[9] R. Carfantan and J. Idier, "Statistical linear destriping of satellite-based pushbroom-type images," *IEEE Trans. Geosci. Remote Sens.*, vol. 48, no. 4, pp. 1860–1871, Apr. 2010.

[10] H. Shen, W. Jiang, H. Zhang, and L. Zhang, "A piece-wise approach to removing the nonlinear and irregular stripes in MODIS data," *Int. J. Remote Sens.*, vol. 35, no. 1, pp. 44–53. Nov. 2013.

[11] J. Pan and C. Chang, "Destriping of Landsat MSS images by filtering techniques," *Photogramm. Eng. Remote Sens.*, vol. 58, no. 10, pp. 1417–1423, Oct. 1992.

[12] J. Torres and S. Infante, "Wavelet analysis for elimination of striping noise in satellite images," *Opt. Eng.*, vol. 40, no. 7, pp. 1309–1314, Jul. 2001.

[13] J. Chen, H. Xie, Y. Shao, and L. Yang, "Oblique striping removal in remote sensing imagery based on wavelet transform," *Int. J. Remote Sens.*, vol. 27, no. 8, pp. 1717–1723, Apr. 2006.

[14] B. Munch, P. Trtik, F. Marone, and M. Stampanoni, "Stripe and ring artifact removal with combined wavelet-Fourier filtering," *Opt. Exp.*, vol. 17, no. 10, pp. 8567–8591, May 2009.

[15] R. Pande-Chhetri and A. Abd-Elrahman, "De-striping hyperspectral imagery using wavelet transform and adaptive frequency domain filtering," *ISPRS J. Photogramm. Remote Sens.*, vol. 66, no. 5, pp. 620–636, Sep. 2011.

[16] H. Shen and L. Zhang, "A MAP-based algorithm for destriping and inpainting of remotely sensed images," *IEEE Trans. Geosci. Remote Sens.*, vol. 47, no. 5, pp. 1492–1502, May 2009.

[17] M. Bouali and S. Ladjal, "Toward optimal destriping of MODIS data using a unidirectional variational model," *IEEE Trans. Geosci. Remote Sens.*, vol. 49, no. 8, pp. 2924–2935, Aug. 2011.

[18] Y. Chang, L. X. Yan, H. Z. Fang, and H. Liu, "Simultaneous destriping and denoising for remote sensing images with unidirectional total variation and sparse representation," *IEEE Geosci. Remote Sens. Lett.*, vol. 11, no. 6, pp. 1051–1055, Jun. 2014.

[19] G. Zhou, H. Fang, L. Yan, T. Zhang, and J. Hu, "Removal of stripe noise with spatially adaptive unidirectional total variation," *Optik—Int. J. Light Electron Opt.*, vol. 125, no. 12, pp. 2756–2762, Jun. 2014.

[20] H. Zhang, W. He, L. Zhang, and H. Shen, "Hyperspectral image restoration using low-rank matrix recovery," *IEEE Trans. Geosci. Remote Sens.*, vol. 52, no. 8, pp. 4729–4743, Aug. 2014.

[21] M. Aharon, M. Elad, and A. M. Bruckstein, "K-SVD: An algorithm for designing overcomplete dictionaries for sparse representation," *IEEE Trans. Signal Process.*, vol. 54, no. 11, pp. 4311–4322, Nov. 2006.

[22] M. Elad and M. Aharon, "Image denoising via sparse and redundant representations over learned dictionaries," *IEEE Trans. Image Process.*, vol. 15, no. 12, pp. 3736–3745, Dec. 2006.

[23] H. Shen *et al.*, "Missing information reconstruction of remote sensing data: A technical review," *IEEE Geosci. Remote Sens. Mag.*, vol. 3, no. 3, pp. 61–85, Sep. 2015.

[24] L. I. Rudin, S. Osher, and E. Fatemi, "Nonlinear total variation noise removal algorithm," *Phys. D, Nonlinear Dyn.*, vol. 60, no. 1–4, pp. 259–268, Nov. 1992.

[25] M. Figueiredo and J. Bioucas-Dias, "Restoration of Poissonian images using alternating direction optimization," *IEEE Trans. Image Process.*, vol. 19, no. 12, pp. 3133–3145, Dec. 2010.

[26] G. Steidl and T. Teuber, "Removing multiplicative noise by Douglas-Rachford splitting methods," *J. Math. Imag. Vis.*, vol. 36, no. 2, pp. 168–184, Feb. 2010.

[27] X. Yuan and J. Yang, "Sparse and low-rank matrix decomposition via alternating direction methods," *Pac. J. Optim.*, vol. 9, no. 1, pp. 167–180, Jan. 2013.

[28] D. Gabay, "Applications of the method of multipliers to variational inequalities," in *Augmented Lagrangian Methods: Applications to the Solution of Boundary-Value Problems*, M. Fortin and R. Glowinski, Eds. Amsterdam, The Netherlands: North Holland, 1983.

[29] J. Eckstein and D. P. Bertsekas, "On the Douglas-Rachford splitting method and the proximal point algorithm for maximal monotone operators," *Math. Programm.*, vol. 55, no. 1, pp. 293–318, Apr. 1992.

[30] S. Boyd, N. Parikh, E. Chu, B. Peleato, and J. Eckstein, "Distributed optimization and statistical learning via the alternating direction method and multipliers," *Found. Trends Mach. Learn.*, vol. 3, pp. 1–122, Jan. 2011.

[31] D. L. Donoho, "De-noising by soft-thresholding," *IEEE Trans. Inf. Theory*, vol. 41, no. 3, pp. 613–627, May 1995.

[32] T. Blumensath and M. E. Davies, "Iterative thresholding for sparse approximation," *J. Fourier Anal. Appl.*, vol. 14, no. 5, pp. 629–654, Dec. 2008.

[33] Y. Jiao, B. Jin, and X. Lu, "A primal dual active set with continuation algorithm for the $\ell 0$-regularized optimization problem," *Appl. Comput. Harmon. Anal.*, vol. 39, no. 3, pp. 400–426, Nov. 2015.

[34] G. Corsini, M. Diani, and T. Walzel, "Striping removal in MOS-B data," *IEEE Trans. Geosci. Remote Sens.*, vol. 38, no. 3, pp. 1439–1446, May 2000.

[35] Z. Wang, A. C. Bovik, and H. R. Sheikh, "Image quality assessment: From error visibility to structural similarity," *IEEE Trans. Image Process.*, vol. 13, no. 4, pp. 600–612, Apr. 2004.

[36] Z. Wang and A. C. Bovik, "Mean squared error: Love it or leave it?—A new look at signal fidelity measures," *IEEE Signal Process. Mag.*, vol. 26, no. 1, pp. 98–117, Jan. 2009.

[37] G. Smith and P. Curran, "Methods for estimating image signal-to-noise ratio (SNR)," in *Advances in Remote Sensing and GIS Analysis*, P. Atkinson and N. Tate, Eds. Hoboken, NJ, USA: Wiley, 2000, pp. 61–74.

[38] J. E. Nichol and V. Vohora, "Noise over water surfaces in Landsat TM images," *Int. J. Remote Sens.*, vol. 25, no. 11, pp. 2087–2094, Jun. 2004.
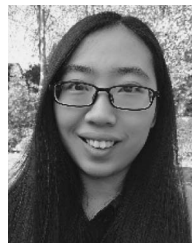
Xinxin Liu received the B.S. degree in geographic information system from Wuhan University, Wuhan, China, in 2013, where she is currently working toward the Ph.D. degree with the School of Resource and Environmental Sciences.

Her research interests include image quality improvement and remote sensing image processing.

Xiliang Lu received the B.S. degree in computational mathematics from Peking University, Beijing, China, in 2000 and the Ph.D. degree in computational mathematics from the National University of Singapore, Singapore, in 2006.

He is currently a Professor with the School of Mathematics and Statistics, Wuhan University, Wuhan, China. His research interests include computational inverse problems and their applications.
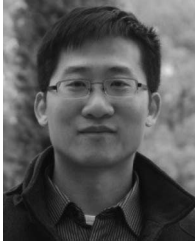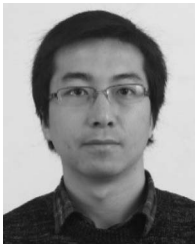
Huanfeng Shen (M'10–SM'13) received the B.S. degree in surveying and mapping engineering and the Ph.D. degree in photogrammetry and remote sensing from Wuhan University, Wuhan, China, in 2002 and 2007, respectively.

In July 2007, he joined the School of Resource and Environmental Sciences, Wuhan University, where he is currently a Luojia Distinguished Professor. He has published more than 100 research papers. His research interests include image quality improvement, remote sensing mapping and application, data fusion and assimilation, and regional and global environmental change.

Dr. Shen is currently a member of the Editorial Board of the *Journal of Applied Remote Sensing*. He has been supported by several talent programs, such as the Youth Talent Support Program of China in 2015, the China National Science Fund for Excellent Young Scholars in 2014, and the New Century Excellent Talents by the Ministry of Education of China in 2011.

Qiangqiang Yuan (M'13) received the B.S. degree in surveying and mapping engineering and the Ph.D. degree in photogrammetry and remote sensing from Wuhan University, Wuhan, China, in 2006 and 2012, respectively.

In 2012, he joined the School of Geodesy and Geomatics, Wuhan University, where he is currently an Associate Professor. He published more than 30 research papers, including more than 20 peer-reviewed articles in international journals such as the IEEE TRANSACTIONS IMAGE PROCESSING and the IEEE TRANSACTIONS ON GEOSCIENCE AND REMOTE SENSING. His current research interests include image reconstruction, remote sensing image processing and application, and data fusion.

Dr. Yuan was the recipient of the Top-Ten Academic Star of Wuhan University in 2011. In 2014, he received the Hong Kong Scholar Award from the Society of Hong Kong Scholars and the China National Postdoctoral Council. He has frequently served as a Referee for more than ten international journals for remote sensing and image processing.

Yuling Jiao received the B.S. degree in applied mathematics from Shangqiu Normal University, Shangqiu, China, in 2008 and the Ph.D. degree in applied mathematics from Wuhan University, Wuhan, China, in 2014.

He is currently a Lecturer with the School of Statistics and Mathematics, Zhongnan University of Economics and Law, Wuhan, China, where he specializes in signal/image processing, inverse problems, and statistical computing.

Liangpei Zhang (M'06–SM'08) received the B.S. degree in physics from Hunan Normal University, Changsha, China, in 1982, the M.S. degree in optics from the Xi'an Institute of Optics and Precision Mechanics, Chinese Academy of Sciences, Xi'an, China, in 1988, and the Ph.D. degree in photogrammetry and remote sensing from Wuhan University, Wuhan, China, in 1998.

He is currently the Head of the Remote Sensing Division, State Key Laboratory of Information Engineering in Surveying, Mapping, and Remote Sensing (LIESMARS), Wuhan University. He is also a Chang-Jiang Scholar Chair Professor appointed by the Ministry of Education of China. He is currently a Principal Scientist for the China State Key Basic Research Project (2011–2016) appointed by the Ministry Of National Science and Technology of China to lead the remote sensing program in China. He has more than 450 research papers and five books. He is the holder of 15 patents. His research interests include hyperspectral remote sensing, high-resolution remote sensing, image processing, and artificial intelligence.

Dr. Zhang is a Fellow of the Institution of Engineering and Technology, an Executive Member (Board of Governors) of the China National Committee of the International Geosphere-Biosphere Programme, an Executive Member of the China Society of Image and Graphics, etc. He received Best Reviewer Awards from the IEEE Geoscience and Remote Sensing Society (GRSS), for his service to the IEEE JOURNAL OF SELECTED TOPICS IN EARTH OBSERVATIONS AND APPLIED REMOTE SENSING (JSTARS) in 2012 and the IEEE GEOSCIENCE AND REMOTE SENSING LETTERS in 2014. He was a recipient of the 2010 Best Paper Boeing Award and the 2013 Best Paper ERDAS Award from the American Society of Photogrammetry and Remote Sensing. His research teams won the top three prizes of the IEEE GRSS 2014 Data Fusion Contest, and his students have been selected as the winners or finalists of the IEEE International Geoscience and Remote Sensing Symposium (IGARSS) Student Paper Contest in recent years. He is the Founding Chair of the IEEE GRSS Wuhan Chapter. He was the General Chair of the 4th IEEE GRSS Workshop on Hyperspectral Image and Signal Processing: Evolution in Remote Sensing (WHISPERS) and a Guest Editor of JSTARS. He regularly serves as a Cochair for the series SPIE Conferences on Multispectral Image Processing and Pattern Recognition, the Conference on Asia Remote Sensing, and many other conferences. He edits several conference proceedings, issues, and geoinformatics symposiums. He also serves as an Associate Editor for the *International Journal of Ambient Computing and Intelligence*, the *International Journal of Image and Graphics*, the *International Journal of Digital Multimedia Broadcasting*, the *Journal of Geo-spatial Information Science*, and the *Journal of Remote Sensing* and as a Guest Editor for the *Journal of Applied Remote Sensing* and the *Journal of Sensors*. He currently serves as an Associate Editor for the IEEE TRANSACTIONS ON GEOSCIENCE AND REMOTE SENSING.